Second-harmonic generation with ultralow-power pump thresholds in a dimer of two active-passive cavities

Jiahua Li,[1,*] Rong Yu,[2,†] Ye Qu,[1] Chunling Ding,[2] Duo Zhang,[3] and Ying Wu[4,‡]

[1]*School of Physics, MOE Key Laboratory of Fundamental Physical Quantities Measurement, Huazhong University of Science and Technology, Wuhan 430074, People's Republic of China*

[2]*School of Science, Hubei Province Key Laboratory of Intelligent Robot, Wuhan Institute of Technology, Wuhan 430205, People's Republic of China*

[3]*School of Electrical and Electronic Engineering, Wuhan Polytechnic University, Wuhan 430023, People's Republic of China*

[4]*Wuhan National Laboratory for Optoelectronics and School of Physics, Huazhong University of Science and Technology, Wuhan 430074, People's Republic of China*

One of the current challenges in second-harmonic generation (SHG) is to increase the efficiency of the second-harmonic conversion process while maintaining or even decreasing the fundamental-harmonic pump powers in a compact device. Here, we put forward an on-chip scheme to realize high-efficiency optical SHG in active-passive-coupled microring resonators with the aid of the intrinsic second-order nonlinearity. By careful analysis and extensive simulations, it is found that the introduction of an active microring resonator makes the strong SHG process feature an ultralow-power pump threshold, which is about four orders of magnitude lower than that in a single-microring resonator SHG system reported previously by X. Guo *et al.* [Optica **3**, 1126 (2016)]. The observed SHG is enhanced by a factor of over 200 compared to the single-microring-resonator SHG system. The SHG conversion efficiency of over 72% can be reached with optical pump power as low as a few microwatts for our proposed device. This investigation may open a new route towards development of easily fabricated radiation sources of coherent high-energy (shorter-wavelength) photons with an ultralow-power laser-triggered SHG process.

I. INTRODUCTION

Second-harmonic generation (SHG) is a kind of nonlinear second-order optical process that attains the frequency conversion of light. Since the first experimental observation of SHG by Franken *et al.* in 1961 [1], SHG has attracted considerable attention and interest because of its potential applications within micron-scale optical structures such as cavities. It is well known that introducing the second-order ($\chi^{(2)}$) nonlinearity is the key basis of the SHG [2–4]. Generally, the intrinsic $\chi^{(2)}$ nonlinearity of existing material systems commonly used for applications in integrated optics is quite weak. In particular, the centrosymmetric lattice structure of unstrained silicon does not permit this second-order optical nonlinearity. Thus, in order to raise the conversion efficiency of the SHG process, long interaction lengths and times and/or strong powers of the input pump field are usually required in devices.

Optical micro- and nanocavities [5,6] in recent years have made great progress, which can provide an ideal material system for reducing the mode volume V, increasing the optical quality factor Q, and further enhancing the nonlinear interaction efficiency [7] at the microscale and nanoscale. In these chip-scalable photonic platforms with the above-mentioned advantages, various microcavity-enhanced SHG schemes (e.g., Fabry-Pérot cavities [8–10], microring cavities [11–14], microdisk cavities [15–18], whispering-gallery-mode resonators [19–25], microbottle resonators [26], and pho-tonic crystal cavities [27–33]) have been demonstrated both theoretically and experimentally by many research groups. However, the achievable SHG efficiency is currently limited by absorption phenomena and is still much lower than the state of the art of the macroscopic resonator [34]. Moreover, the SHG setup needs to be driven with high pump power for achieving large conversion efficiency in this process [14].

Then, a corresponding question arises: is it possible to optimize the configuration design (e.g., an active microring resonator is introduced to form an active-passive-coupled microring-resonator SHG dimer structure, rather than a single-passive-microring-resonator SHG system [14]) so that optical SHG efficiency can be significantly enhanced for low enough pump power? The answer is yes. More recently, it was clearly shown that the active cavities can be extensively employed to improve the sensitivity and precision of detection of nanoparticles [35], to improve the monitoring of scatterer-induced mode splitting [36], to extend photon lifetimes to the millisecond range (lifetimes that are characteristic of phonons) [37], to manipulate slow and fast light and dynamic pulse splitting [38], to control dynamic Fano-like resonances [39], to amplify a higher-order sideband [40], and to constitute parity-time ($\mathcal{PT}$)-symmetric microcavities (for recent reviews, see, e.g., Ref. [41] and references therein), including $\mathcal{PT}$-symmetric lasers [42–46] and nonreciprocal light transmission [47,48], together with other interesting physical phenomena [49–52]. Thus, the active-cavity-assisted devices may be a rich playground to significantly boost SHG processes, which have not been reported so far.

Motivated by the studies above, in the present work we theoretically propose and investigate in detail an on-chip scheme to efficiently enhance the SHG via an integrated

---

*huajia_li@163.com

†rong_yu2013@126.com

‡yingwu2@126.com

nonlinear optical system based on the active-passive-coupled double-microring resonators. By pumping the device with a continuous-wave laser (seed) near the fundamental-harmonic (FH) mode at the telecommunication wavelength, it is clearly shown that the strong SHG process can exhibit the following three important aspects.

First of all, the incident pump powers are rather low. Even if an ultralow-power-driving pump is applied, an intense SHG can be triggered in an active-cavity-assisted SHG dimer system. It is found that the pump power required here is more than four orders of magnitude lower than that in a standard single-cavity SHG system reported previously [11–14].

Second, the efficiency of the SHG is large. In this proposed microring dimer configuration, the observed SHG is enhanced by factor of over 200 compared to the single-microring-resonator SHG system reported previously by Guo *et al.* [14]. At the same time, the SHG conversion efficiency of around 72% can be obtained for a pump power of as low as 5 μW.

Third, the size of the SHG dimer system is small. The significantly compact device proposed here can be combined with integrated photonic chips, which are very robust and scalable. In other words, compared with the previous studies [11–18], our study achieved considerable improvement of the nonlinear conversion efficiency that may pave the way for practical applications using low-power nonlinear SHG-based all-optical signal processing on chip.

The structure of this paper is as followings. We present our model and the corresponding dynamical equations of motion in Sec. II. Subsequently, the formal solutions of the coupled equations are given in the steady-state case. In Sec. III, we briefly illustrate the choice of a set of typical system parameters found experimentally in microring resonators and experimental feasibility. In Sec. IV, we analyze and discuss how highly efficient SHG can be achieved with ultralow pump driving by using experimentally accessible parameters. Also, the influences of the detunings on the SHG are analyzed in detail. Finally, we conclude the paper in Sec. V.

II. PHYSICAL MODEL, HAMILTONIAN, EQUATIONS OF MOTION, AND SOLUTIONS

Referring to the schematic in Fig. 1 for the SHG process, we consider a dimer configuration comprising two coupled passive-active microring resonators. An optical passive (loss) microring resonator with second-order nonlinearity $\chi^{(2)}$ possesses two optical modes, one mode at the FH frequency (represented by $\hat{a}$ and ω_a) and another mode at the second-harmonic (SH) frequency (represented by $\hat{b}$ and $\omega_b \simeq 2\omega_a$). In this $\chi^{(2)}$-type microring structure, the second-order nonlinear optical process relates two photons at the FH frequency to a photon at the SH frequency, which mediates a nonlinear coherent interaction (represented by g) between the two different frequencies, ω_a and ω_b. We refer the reader to Refs. [3,14] and references therein for more details on the specific realization of such dual-resonant $\chi^{(2)}$-type microcavities. At the same time, an additional active (gain) single-mode microring resonator (represented by $\hat{c}$) with a resonance frequency $\omega_c \simeq \omega_a$ is used to evanescently couple the FH mode $\hat{a}$ of the passive microring resonator via their spectral overlap [43–48], with a coupling strength J. The
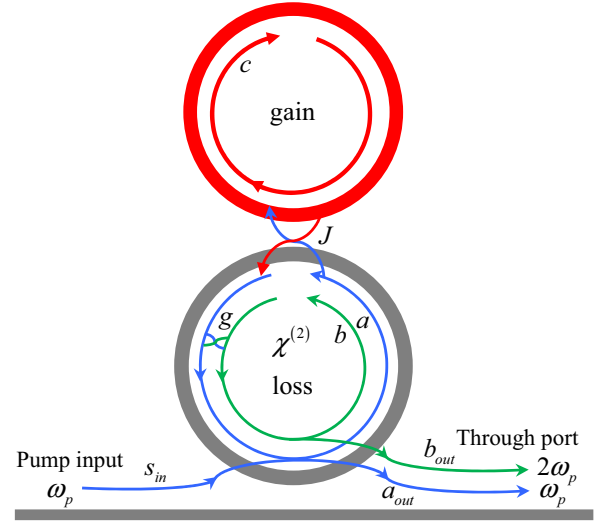

FIG. 1. Schematic for the enhanced SHG process in the coupled-resonator system under study. An optical passive (loss) microring resonator with the second-order nonlinearity $\chi^{(2)}$ (the gray ring) involves two optical modes, one mode at the FH frequency ω_a (blue line) and another mode at the SH frequency $\omega_b \simeq 2\omega_a$ (green line). At the same time, the FH mode of the passive $\chi^{(2)}$-type microring resonator is evanescently coupled to an active (gain) microring resonator ($\omega_c \simeq \omega_a$, the red ring) with a coupling strength J. A pump field near the FH frequency ($\omega_p \simeq \omega_a$) is applied on the passive microring resonator to drive its FH mode through a side-coupled waveguide (e.g., a fiber taper; gray straight line).

dynamics of the whole waveguide-side-coupled dimer system with the pump-light driving near the FH frequency ($\omega_p \simeq \omega_a$) can be described by the Hamiltonian

$$\hat{H} = \hat{H}_0 + \hat{H}_{ab} + \hat{H}_{ac} + \hat{H}_{dri}. \tag{1}$$

The first term describes the energies of the three cavity modes in the absence of the intermode coupling and is given by

$$\hat{H}_0 = \hbar\omega_a \hat{a}^\dagger \hat{a} + \hbar\omega_b \hat{b}^\dagger \hat{b} + \hbar\omega_c \hat{c}^\dagger \hat{c}, \tag{2}$$

where $\hat{a}$ ($\hat{a}^\dagger$), $\hat{b}$ ($\hat{b}^\dagger$), and $\hat{c}$ ($\hat{c}^\dagger$) are the annihilation (creation) operators of the FH, SH, and active photonic modes with the commutation relations $[\hat{a}, \hat{a}^\dagger] = 1$, $[\hat{b}, \hat{b}^\dagger] = 1$, and $[\hat{c}, \hat{c}^\dagger] = 1$, respectively.

The second term in Eq. (1) describes a coupling of the FH mode with the SH mode through the second-order nonlinearity $\chi^{(2)}$ in the passive microring resonator, which converts two photons at the FH frequency to a photon at the SH frequency:

$$\hat{H}_{ab} = \hbar g[\hat{a}^2 \hat{b}^\dagger + (\hat{a}^\dagger)^2 \hat{b}], \tag{3}$$

where g is a nonlinear coupling constant between the two modes whose explicit expression is provided in detail in Ref. [14], with the following form:

$$g = \zeta \sqrt{\frac{\hbar\omega_a^2 \omega_b}{\epsilon_0 2\pi R}} \frac{1}{\epsilon_a \sqrt{\epsilon_b}} \frac{3\chi^{(2)}}{4\sqrt{2}}, \tag{4}$$

where the geometrical parameters involved are the radius of the passive microring R and the effective mode-overlapping factor at the cross section of the microring ζ. As a result, in order to achieve a large nonlinear coupling constant g, a large overlap

of the FH and SH modes of the microring resonator has to be attained through intracavity photothermal tuning [14,18]. This formula also emphasizes that a material with a high second-order susceptibility coefficient $\chi^{(2)}$, small microring radius R, and low relative permittivity of dielectrics $\epsilon_{a(b)}$ is preferable. Above, ϵ_0 is the vacuum permittivity.

The third term in Eq. (1) describes the coupling of the FH mode in the $\chi^{(2)}$-type microring resonator with the single mode in the active microring resonator:

$$\hat{H}_{ac} = \hbar J(\hat{a}\hat{c}^\dagger + \hat{a}^\dagger\hat{c}). \tag{5}$$

Notice that the intercavity coupling strength J can be tuned and controlled by the gap between the two microring resonators, as shown experimentally in Refs. [43–48]. It is also worthwhile to mention that, in the limit of vanishing value $J = 0$, the proposed model reduces to the standard Hamiltonian of the single-microring-resonator SHG system in Ref. [14].

Finally, the last term in Eq. (1) describes an external driving field pumping the FH mode:

$$\hat{H}_{dri} = \hbar\sqrt{\eta_a\kappa_a}(\varepsilon_p\hat{a}^\dagger e^{-i\omega_p t} + \varepsilon_p^*\hat{a}e^{i\omega_p t}), \tag{6}$$

where the input pump field can be expressed by $s_{in}(t) = \varepsilon_p e^{-i\omega_p t}$, with the drive frequency ω_p and field amplitude ε_p related to the pump power P_p by the relationship $\varepsilon_p = \sqrt{P_p/(\hbar\omega_p)}$. The cavity-waveguide coupling coefficient η_a for the FH mode is given by $\eta_a = \kappa_e^a/(\kappa_a^i + \kappa_a^e) = \kappa_a^e/\kappa_a$, where κ_a^i, κ_a^e, and $\kappa_a \equiv \kappa_a^i + \kappa_a^e$ denote the intrinsic, external, and total loss rates, respectively. The former (κ_a^i) is due to loss in the resonator itself, whereas the latter (κ_a^e) is due to the coupling to the waveguide. Similarly, $\eta_b = \kappa_e^b/(\kappa_b^i + \kappa_b^e) = \kappa_b^e/\kappa_b$, where κ_a^i, κ_a^e, and $\kappa_b \equiv \kappa_b^i + \kappa_b^e$ denote the intrinsic, external, and total decay rates of the SH mode, respectively. In the following, for the active microring resonator, κ_c denotes its effective loss rate, which is reduced by the external pump ξ [35–40] with the relationship $\kappa_c = \kappa_c^i - \xi$ (κ_c^i is the intrinsic loss rate of the cavity mode $\hat{c}$). It is obvious that $\kappa_c > 0$ corresponds to a passive cavity, and in contrast, $\kappa_c < 0$ corresponds to an active one.

Applying a unitary transformation (or, equivalently, a reference frame rotating with pump frequency ω_p) $\hat{U} = \exp[-i\omega_p t(\hat{a}^\dagger\hat{a} + 2\hat{b}^\dagger\hat{b} + \hat{c}^\dagger\hat{c})]$, we transform the Hamiltonian (1) into the form (assuming $\hbar = 1$)

$$\hat{\mathcal{H}}_{rot} = \Delta_a\hat{a}^\dagger\hat{a} + \Delta_b\hat{b}^\dagger\hat{b} + \Delta_c\hat{c}^\dagger\hat{c} + J(\hat{a}\hat{c}^\dagger + \hat{a}^\dagger\hat{c})$$
$$+ g[\hat{a}^2\hat{b}^\dagger + (\hat{a}^\dagger)^2\hat{b}] + \sqrt{\eta_a\kappa_a}(\varepsilon_p\hat{a}^\dagger + \varepsilon_p^*\hat{a}), \tag{7}$$

where $\Delta_a = \omega_a - \omega_p$, $\Delta_b = \omega_b - 2\omega_p$, and $\Delta_c = \omega_c - \omega_p$ are the frequency detunings of the FH, SH, and active modes from the pump laser. For most of this paper, we study the situation $\omega_b = 2\omega_a$; thus, we have $\Delta_b = 2\Delta_a$. When considering their detuning $W = \omega_b - 2\omega_a$, we have the relationship $\Delta_b = 2\Delta_a + W$. In addition, when setting the detuning $\Omega = \omega_c - \omega_a$ between the active and FH modes, we have the relationship $\Delta_c = \Delta_a + \Omega$.

According to the resulting Hamiltonian [Eq. (7)] and Heisenberg-Langevin formalism $\frac{d\hat{F}}{dt} = -i[\hat{F}, \hat{\mathcal{H}}_{rot}]$, reducing the operators to their mean values and dropping the quantum noise terms (all the noise operators have zero mean values), we can arrive at the following Heisenberg-Langevin equations

of motion:

$$\frac{da}{dt} = -(i\Delta_a + \kappa_a/2)a - iJc - 2iga^*b - i\sqrt{\eta_a\kappa_a}\varepsilon_p, \tag{8}$$

$$\frac{db}{dt} = -(i\Delta_b + \kappa_b/2)b - iga^2, \tag{9}$$

$$\frac{dc}{dt} = -(i\Delta_c + \kappa_c/2)c - iJa, \tag{10}$$

where the decay rates (κ_a, κ_b, and κ_c) of the FH, SH, and active-cavity modes have been added phenomenologically [53,54].

The formal solutions of Eqs. (8)–(10) in the steady-state condition by setting all the time derivatives to zero (i.e., $\frac{dx}{dt} = 0$, $x = a, b, c$) can be obtained as

$$h_3|a|^6 + h_2|a|^4 + h_1|a|^2 + h_0 = 0, \tag{11}$$

$$b = \frac{-iga^2}{\delta_b}, \tag{12}$$

$$c = \frac{-iJa}{\delta_c}, \tag{13}$$

where we have defined the following coefficients:

$$h_0 = -\eta_a\kappa_a|\delta_b|^2|\delta_c|^2\varepsilon_p^2, \tag{14}$$

$$h_1 = |\delta_b|^2[|\delta_a|^2|\delta_c|^2 + (\delta_a\delta_c + \delta_a^*\delta_c^*)J^2 + J^4], \tag{15}$$

$$h_2 = 2g^2[(\delta_a\delta_b + \delta_a^*\delta_b^*)|\delta_c|^2 + (\delta_b\delta_c^* + \delta_b^*\delta_c)J^2], \tag{16}$$

$$h_3 = 4|\delta_c|^2g^4, \tag{17}$$

together with $\delta_a = i\Delta_a + \kappa_a/2$, $\delta_b = i\Delta_b + \kappa_b/2$, and $\delta_c = i\Delta_c + \kappa_c/2$. It is pointed out that, for Eq. (11), the numerical calculation is needed to solve the value of a.

By means of the connection between the Heisenberg-Langevin equation formalism and the input-output theory [53,54], namely, the relation $b_{out} = -i\sqrt{\eta_b\kappa_b}b$ for the SHG process, we can arrive at the intensity transmission of the SH signal, which is the absolute-value square of the ratio of the SH output field to the input pump field, as follows:

$$T_b = \left|\frac{b_{out}}{\varepsilon_p}\right|^2 = \frac{\eta_b\kappa_b|b|^2}{\varepsilon_p^2} = \frac{\eta_b\kappa_b g^2|a|^4}{|\delta_b|^2\varepsilon_p^2}, \tag{18}$$

where b_{out} is the field amplitude of the output SH signal. Equation (18) also yields the absolute conversion efficiency of the SH signal. It is an important figure of merit to evaluate the SHG conversion performance.

III. CHOICE OF TYPICAL PARAMETERS FOUND EXPERIMENTALLY IN MICRORING RESONATORS AND EXPERIMENTAL FEASIBILITY

Before proceeding, we briefly address the state-of-the-art parameter set for the numerical simulations. Here, we make use of typical experimental parameter values for the dual-resonant aluminum nitride (AlN) microring resonator reported in Ref. [14], where the intrinsic $\chi^{(2)}$-type nonlinearity and the coupling conditions for dual-band operation can be precisely controlled with nanofabrication technology and the phase-matching conditions can be fulfilled through thermal

tuning. According to the experiment in Ref. [14], a nonlinear coupling strength via second-order nonlinearity $\chi^{(2)}$ can be made to be $g/2\pi \sim 0.1$ MHz. The actual values of the other system parameters in the relevant experiment [14] are chosen for the microring resonator to be the FH mode wavelength $\lambda_a = 1550$ nm, the SH mode wavelength $\lambda_b = 775$ nm, the total quality factor of FH mode $Q_a = 4.6 \times 10^5$ [corresponding to the total loss rate $\kappa_a/2\pi = c/(\lambda_a Q_a) \simeq 0.4$ GHz], the total quality-factor of SH mode $Q_b = 2.3 \times 10^5$ [corresponding to the total loss rate $\kappa_b/2\pi = c/(\lambda_b Q_b) \simeq 1.7$ GHz], and the cavity-waveguide coupling coefficients $\eta_a = 0.5$ for the FH mode and $\eta_b = 0.75$ for the SH mode. We set the intercavity coupling strength $J/2\pi = 0.18$ GHz without loss of generality, which can be readily achieved by adjusting the gap between the two microring resonators [43–48]. The active resonator is fabricated from rare-earth-ion (e.g., Er^{3+}) doped silica, and the gain is provided by optical pumping [43–48]. An individual bus waveguide with the add-through configuration fabricated by the heat-and-pull technique is used to guide laser light into and out of the FH and SH modes of the passive microring resonator.

Subsequently, we give a brief discussion of the more technical aspects regarding the experimental feasibility of this double-microring-resonator system (see Fig. 1). First, the passive microring resonator is made from AlN [14], whereas the active microring resonator is made from erbium-ion-doped silica film, which is formed using sol-gel synthesis [47]. The coupling strength is tuned by varying the distance between the two microring resonators. A natural question to ask, then, is how both the Er-doped active microring and the AlN passive microring are put on the same epitaxial chip by respecting the design distance between them. This can be done by fabricating each of the microrings at the edge of a different chip and by controlling the separation between chips by using nanopositioning systems on which the chips are placed. This is a technique that has been successfully employed in Refs. [47,55].

Second, it has been experimentally shown in Refs. [14,56] that the energy conservation or, equivalently, the wavelength matching ($\omega_b = 2\omega_a$ or $\lambda_a = 2\lambda_b$) can be roughly satisfied by engineering the width of the microring appropriately. That is to say, the resonance wavelength of the FH mode a is roughly 2 times that of the SH mode b, with a small misalignment. In this case, the small misalignment means that the energy conservation is not perfectly fulfilled. In order to optimize SHG efficiency, therefore, we need to finely tune the two resonances to perfectly fulfill the energy conservation condition via thermal tuning [14,47,55]. As expected, the optimized SHG efficiency will occur at a certain temperature when the energy conservation condition holds. The quantitative influence of thermal tuning on the SHG behavior is beyond the scope of the current work and will be systematically explored in the future.

Last, on the one hand, as is well known, only when the frequencies of the two cavity modes [e.g., (i) the FH mode a and the active mode c in the form of the linear exchange-type coupling, see Eq. (5), or (ii) the FH mode a and the SH mode b in the form of the nonlinear double-frequency coupling, see Eq. (3)] are the same (resonance) or close (near resonance) does a strong coherent interaction between both modes appear. Mathematically, this condition is expressed as $\omega_a \simeq \omega_c$ for

case (i) and $\omega_b \simeq 2\omega_a$ for case (ii). It is worth mentioning that the frequency of the SH mode b is roughly 2 times that of the active mode c in the proposed scheme because the frequencies of the two cavity modes (i.e., the FH mode a and the active mode c) are the same (at resonance) or close (near resonance), i.e., $\omega_a \simeq \omega_c$ via thermal tuning. At the same time, the frequency of the SH mode b is 2 times that of the FH mode a, i.e., $\omega_b \simeq 2\omega_a$ via thermal tuning. As a consequence, cavity modes b and c can be well decoupled owing to a large frequency space with a value of $\sim\omega_a$. On the other hand, the nonlinear $\chi^{(2)}$-type material between the passive microring and the active microring does not exist at all, which also avoids the nonlinear optical response of the intercavity coupling at the SH wavelength. Overall, we believe that the present model can provide a qualitative illustration of the following observable SHG properties.

IV. RESULTS AND DISCUSSION FOR ACTIVE-PASSIVE RESONATOR-ENHANCED SHG

We now numerically calculate the SHG intensity based on Eqs. (11)–(13) and (18). Figure 2(a) shows the normalized intensity transmission spectra of the SH signal for three different characteristic configurations: (i) a single-microring-resonator SHG system (the blue dashed line) from [14], (ii) a passive-microring-resonator-assisted SHG dimer system (the pink dotted line), and (iii) an active-microring-resonator-assisted SHG dimer system (the red solid line). First of all, we find from the blue dashed line in Fig. 2(a) that, for a single-microring-resonator SHG system, the SHG T_b slightly increases as P_p quickly increases and T_b is weak. Second, for a passive-microring-resonator-assisted dimer system, the SHG follows a trend similar to that in the previous case in a single-microring-resonator SHG system, as shown by the pink dotted line in Fig. 2(a). Nevertheless, the SHG becomes increasingly weaker. Last, it can be easily seen from the red solid line in Fig. 2(a) that, in an active-microring-resonator-assisted SHG dimer system, there is a significant enhancement of the SHG compared with the other two configurations. In particular, the intensity of the SHG grows much faster than the other two for low enough pump. Specifically, as the pump power P_p is increased, the SHG T_b grows considerably, and then it saturates, and an obvious SHG peak appears in the transmission spectra. With further increasing P_p, T_b starts to drop slowly, but it still is much larger than in the other two cases. The high SHG transmission intensities (also representing the conversion efficiencies) of 50%, 72%, and 86% can be achieved at pump powers of 2, 5, and 10 μW, respectively. The SHG transmission T_b is maximized at $P_p \simeq 35$ μW with the value $T_b \simeq 1$ [see Fig. 2(a)].

The reason for the saturation and reduction effects [see Fig. 2(a)] in the SHG intensity against the pump field in the active-microring-resonator-assisted SHG dimer system can be well explained as follows. With high pump power, the non-negligible back-action of the SH field on the FH field gives rise to an optical stimulated down-conversion process, which corresponds to the term $-2iga^*b$ in Eq. (8) [57]. The interference and competition between the SH field and the stimulated down-conversion therefore leads to the saturation to reduction of the SH photon output [3]. Actually, the
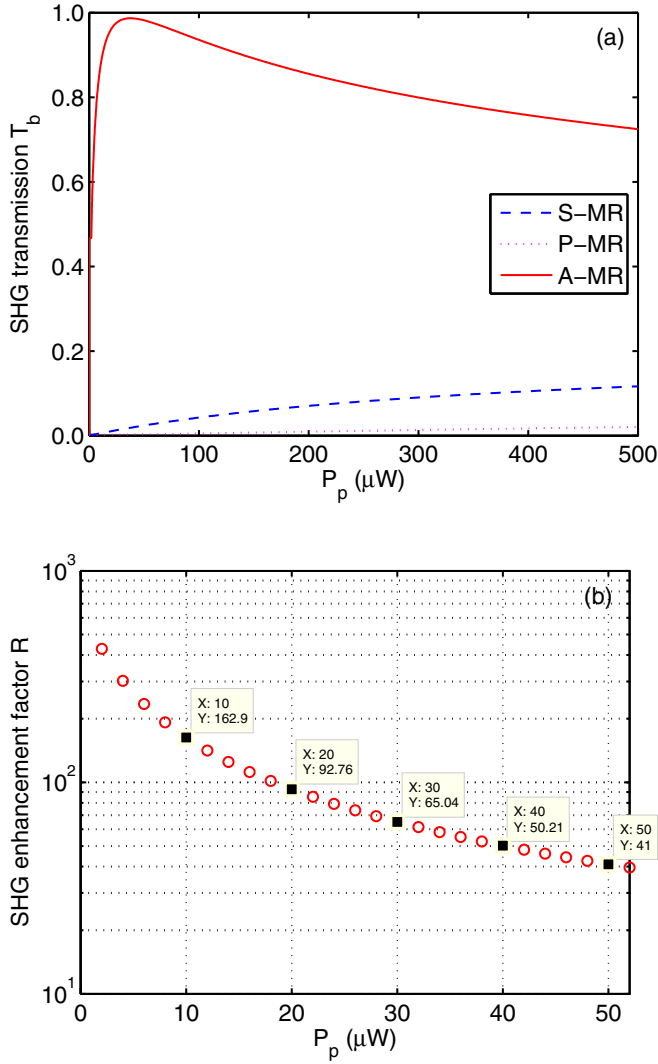
FIG. 2. (a) Normalized SHG intensity transmission T_b as a function of the FH pump power P_p for three different characteristic configurations: (i) a single-microring-resonator (S-MR) SHG system ($J/2\pi = 0$ and $\kappa_c/2\pi = 0$), (ii) a passive microring resonator (P-MR) assisted SHG dimer system ($J/2\pi = 0.18$ GHz and $\kappa_c/2\pi = 0.4$ GHz), and (iii) an active microring resonator (A-MR) assisted SHG dimer system ($J/2\pi = 0.18$ GHz and $\kappa_c/2\pi = -0.4$ GHz). Here, T_b is normalized to the input pump intensity. (b) SHG enhancement factor R, defined by $R = T_b^{(A-MR)}/T_b^{(S-MR)}$, versus the FH pump power P_p. Other system parameters are chosen to be $g/2\pi = 0.1$ MHz, $\kappa_a/2\pi = 0.4$ GHz, $\kappa_b/2\pi = 1.7$ GHz, $\eta_a = 0.5$, $\eta_b = 0.75$, $W/2\pi = 0$, $\Delta_a/2\pi = 0$, $\Delta_b/2\pi = 0$, and $\Delta_c/2\pi = 0$. The wavelength of the FH pump field is chosen to be $\lambda_p = 1550$ nm.

single-microring-resonator SHG system reported previously in [14] also exhibits this typical saturation-to-reduction property in the significantly strong pump regime corresponding to a few tens of milliwatts, which is about four orders of magnitude higher than the several microwatts required in the present active-microring-resonator-assisted SHG dimer system.

In order to further evaluate the enhancement degree of the SHG process in an explicit way, we define a SHG enhancement factor, quantified by $R = T_b^{(A-MR)}/T_b^{(S-MR)}$, which is the ratio of the SHG intensity from our proposed active-microring-resonator-assisted SHG dimer system to that

from the previous single-microring-resonator SHG system in Ref. [14]. Figure 2(b) clearly displays the SHG enhancement factor R against the pump power P_p. We observe from Fig. 2(b) that, when the pump power P_p is set equal to the value of 10 μW in this simulation, there is as much as a 163-fold enhancement of the SHG compared to that reported by the single-microring-resonator SHG system in Ref. [14]. As P_p increases, R becomes smaller, but still $R \gg 1$, e.g., $R = 41$ for $P_p = 50$ μW, as shown in Fig. 2(b).

Moreover, from Fig. 2 another noteworthy feature can be found; that is, the obtained SHG allows an ultralow pump threshold for such an active-microring-resonator-assisted SHG dimer system. For example, we can achieve the SHG intensity $T_b \simeq 0.72$–8.85 in the weak-driving regime corresponding to the ultralow pump power $P_p = 5$–10 μW. To gain important physical insights into the feature of this ultralow pump threshold in the strong SHG response, we follow the approach in Ref. [14] to introduce the SHG cooperativity parameter β by the relation $\beta = 8g^2|a|^2/(\kappa_a\kappa_b)$, which is directly proportional to $|a|^2$ (note that, here, $|a|^2$ stands for the intracavity energy of the FH mode). This means that the cooperativity parameter β can measure the intracavity energy of the FH mode in the passive microring resonator. The intracavity energy at FH is increased gradually by the pump field from external driving and the coupling of the second active microring. When the intracavity energy at FH is enough strong, the FH intracavity field and the down-conversion can cancel due to the interference between them [3,14], leading to a saturation of the SHG intensity transmission and thereafter its depletion. So there exists a maximum SHG intensity transmission at a specific input power, which is called the threshold pump power.
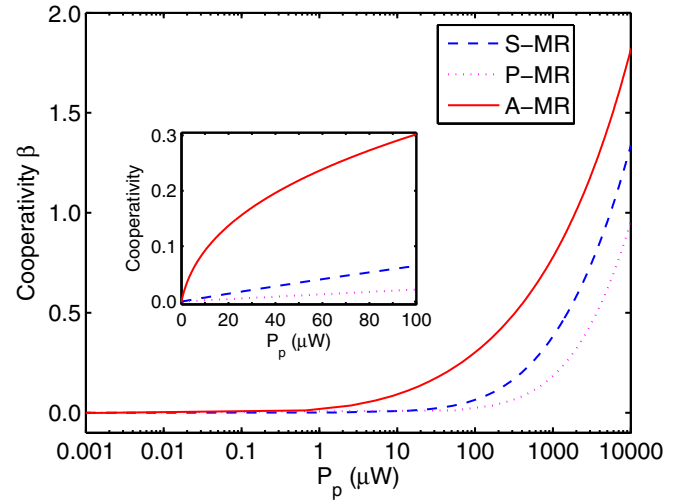

FIG. 3. Cooperativity β for the SHG process against the FH pump power P_p for three different characteristic configurations: (i) a single-microring-resonator (S-MR) SHG system ($J/2\pi = 0$ and $\kappa_c/2\pi = 0$), (ii) a passive microring resonator (P-MR) assisted SHG dimer system ($J/2\pi = 0.18$ GHz and $\kappa_c/2\pi = 0.4$ GHz), and (iii) an active microring resonator (A-MR) assisted SHG dimer system ($J/2\pi = 0.18$ GHz and $\kappa_c/2\pi = -0.4$ GHz). In the inset we show an enlarged view of the cooperativity parameter for clarity. The parameters used for the calculation are $g/2\pi = 0.1$ MHz, $\kappa_a/2\pi = 0.4$ GHz, $\kappa_b/2\pi = 1.7$ GHz, $\eta_a = 0.5$, $\eta_b = 0.75$, $W/2\pi = 0$, $\Delta_a/2\pi = 0$, $\Delta_b/2\pi = 0$, and $\Delta_c/2\pi = 0$.
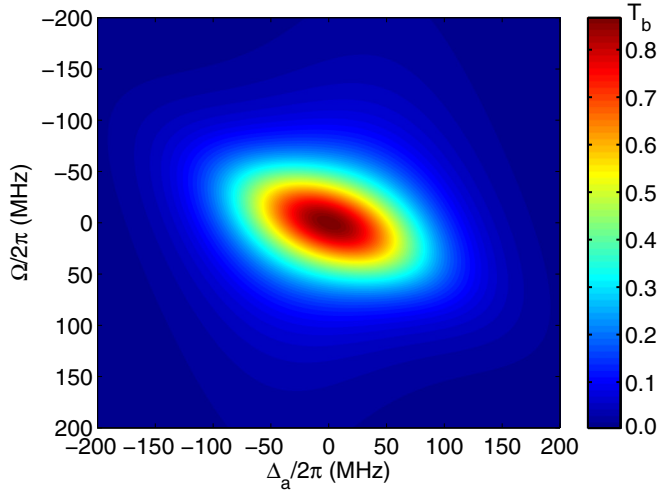
FIG. 4. Contour plot of the normalized SHG intensity transmission T_b as a function of the detuning Δ_a between the pump field and FH mode as well as the detuning Ω between the active-cavity mode and FH mode for the active-microring-resonator-assisted SHG dimer system. Other system parameters are $g/2\pi = 0.1$ MHz, $J/2\pi = 0.18$ GHz, $\kappa_a/2\pi = 0.4$ GHz, $\kappa_b/2\pi = 1.7$ GHz, $\kappa_c/2\pi = -0.4$ GHz, $\eta_a = 0.5$, $\eta_b = 0.75$, $W/2\pi = 0$, and $P_p = 10\,\mu$W.

In Fig. 3, we present the dependence of the SHG co-operativity parameter β on the pump power P_p for three different configurations corresponding to Fig. 2(a). The inset in Fig. 3 shows the expanded spectra in a smaller region of the vertical axis. Note that the blue dashed line in Fig. 3 for the single-microring-resonator SHG system in [14] corresponds to Fig. S1 of Ref. [58]. It is easy to see from Fig. 3 that the SHG cooperativity parameter β can be enhanced significantly for the active-microring-resonator-assisted SHG dimer system with respect to the other two cases. Specifically, the SHG
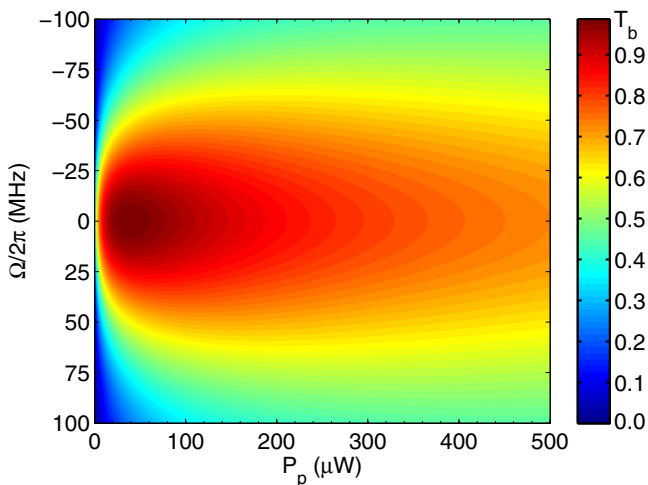

FIG. 5. Contour plot of the normalized SHG intensity transmission T_b as a function of the FH pump power P_p and the detuning Ω between the active-cavity mode and FH mode for the active-microring-resonator-assisted SHG dimer system. Other system parameters are $g/2\pi = 0.1$ MHz, $J/2\pi = 0.18$ GHz, $\kappa_a/2\pi = 0.4$ GHz, $\kappa_b/2\pi = 1.7$ GHz, $\kappa_c/2\pi = -0.4$ GHz, $\eta_a = 0.5$, $\eta_b = 0.75$, $W/2\pi = 0$, and $\Delta_a/2\pi = 0$.
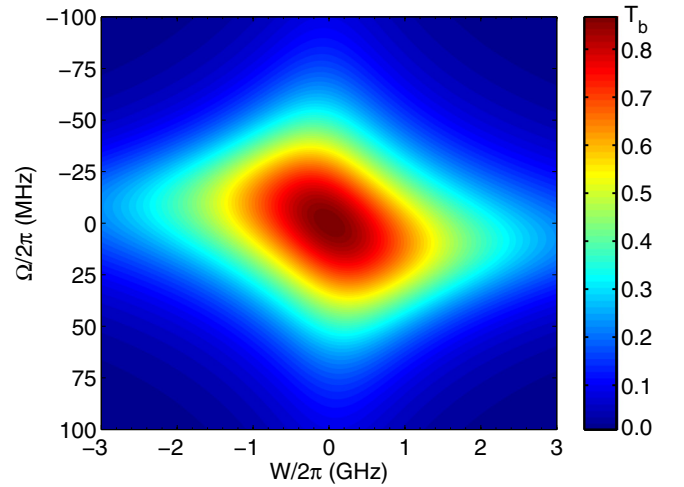

FIG. 6. Contour plot of the normalized SHG intensity transmission T_b as a function of the detuning Δ_a between the pump field and FH mode as well as the detuning W between the SH mode and FH mode for the active-microring-resonator-assisted SHG dimer system. Other system parameters are $g/2\pi = 0.1$ MHz, $J/2\pi = 0.18$ GHz, $\kappa_a/2\pi = 0.4$ GHz, $\kappa_b/2\pi = 1.7$ GHz, $\kappa_c/2\pi = -0.4$ GHz, $\eta_a = 0.5$, $\eta_b = 0.75$, $\Delta_a/2\pi = 0$, and $P_p = 10\,\mu$W.

cooperativity parameter β for a pump power of 20 μW is around 0.014 at the single-microring-resonator SHG system and 0.004 at the passive-microring-resonator-assisted SHG dimer system, while it is enhanced by 10 to 35 times up to 0.14 with the active-microring-resonator-assisted SHG dimer system, as shown in the inset of Fig. 3.

Physically, for our considered dimer configuration consisting of two loss-gain microring resonators, the efficient FH field localization can occur by introducing the second gain microring resonator owing to the linear exchange-type coupling between the FH mode a and the active mode c [see Eq. (5)]. This process efficiently induces dynamical accumulation of the intracavity energy at the FH mode in the $\chi^{(2)}$-type passive microring resonator as depicted in Fig. 3, which thus produces a greatly enhanced $\chi^{(2)}$ nonlinearity (see [59–63] and references therein). This ultimately leads to the observed results that the SHG efficiency is enhanced and the SHG is triggered even if an ultralow pump power is applied.

In the analysis so far, however, we have not yet taken into account the frequency detunings including (i) Δ_a between the pump field and the FH mode, (ii) Ω between the active-cavity mode and the FH mode, and (iii) W between the SH mode and the FH mode introduced in Eq. (7) when calculating the SHG intensity. To this end, we now discuss the influences of Ω, Δ_a, and W on the SHG intensity for the active-microring-resonator-assisted SHG dimer system, as shown in Figs. 4–6. In Fig. 4, we plot the two-dimensional color-scale map of the SHG intensity transmission T_b as a function of the detuning Δ_a between the pump field and the FH mode as well as the detuning Ω between the active-cavity mode and the FH mode. The FH pump power in Fig. 4 is fixed at a value of 10 μW. We immediately see from Fig. 4 that the SHG intensity transmission spectrum is modified dynamically by the presence of the detunings Δ_a and Ω, regardless of the sign of these detunings. Specifically, the SHG intensity

T_b decreases rapidly with the increase in both Δ_a and Ω. Physically, this is because, on the one hand, the second-order nonlinearity-induced interactions become weakened under the off-resonance pump powers and, on the other hand, the localization-induced intensity accumulation in the $\chi^{(2)}$-type passive microring resonator is heavily suppressed under the off-resonance intercavity coupling intensities. In other words, in the existence of these nonzero-frequency detunings, the key consequence is that the second nonlinear process becomes less efficient in a sense.

In order to further show explicitly the dependency of the generated SH output spectrum on the detuning Ω and the pump power P_p, we plot the density distribution of the SHG intensity transmission in Fig. 5 under the condition of the detuning $\Delta_a = 0$. As is seen from the color plot, this SHG phenomenon can be triggered even though a small amount of pump power is applied to the system. For given intrinsic resonator parameters like quality factors and second-order nonlinearity, therefore, the SHG can be optimized by choosing the appropriate pump power and vanishing frequency detuning. These results are consistent with those obtained from Fig. 2(a). Finally, Fig. 6 represents the contour diagram showing the intensity variation of the SH transmitted field with respect to the detuning W between the SH mode and the FH mode as well as the detuning Ω between the active-cavity mode and the FH mode under $\Delta_a = 0$. As shown in Fig. 6, characteristics similar to those in Fig. 4 can be observed as W increases.

V. CONCLUDING REMARKS

In summary, we have proposed and explored an efficient and low-power SHG process in a compact dimer configuration by utilizing currently available technology within the framework of quantum optics. Here, the hybrid system comprises the active-passive double-microring resonators with the effective $\chi^{(2)}$ nonlinearity of the AlN material. By making the passive microring resonator doubly resonant at a FH wavelength of 1500 nm (*C* band) and a SH wavelength of 750 nm (visible range), the SHG intensity transmission can be enhanced by a factor of over 200 due to the presence of an active microring resonator for our device compared with the previous result in a single-microring-resonator SHG scheme [14]. A SHG efficiency of about 72% is predicted for a pump power of as low as 5 μW. At the same time, it turns out that the strong SHG process features an ultralow-power pump threshold, which, to our knowledge, was not possible before in a single-microring-resonator SHG system. The frequency-doubling scheme demonstrated here may provide a potential route for development of a new tunable laser source of coherent high-energy photons with a microwatt-level threshold on a chip. We believe that our proposal is feasible in experimental realizations and deserves to be tested with the currently existing experimental conditions.

[1] P. A. Franken, A. E. Hill, C. W. Peters, and G. Weinreich, Generation of Optical Harmonics, Phys. Rev. Lett. **7**, 118 (1961).

[2] R. W. Boyd, *Nonlinear Optics*, 3rd ed. (Academic, Oxford, 2008).

[3] Z. Lin, X. Liang, M. Lončar, S. G. Johnson, and A. W. Rodriguez, Cavity-enhanced second-harmonic generation via nonlinear-overlap optimization, Optica **3**, 233 (2016). Also see the corresponding supplementary information.

[4] H. Jung and H. X. Tang, Aluminum nitride as nonlinear optical material for on-chip frequency comb generation and frequency conversion, Nanophotonics **5**, 263 (2016), and references therein.

[5] K. J. Vahala, *Optical Microcavities* (World Scientific, Hackensack, NJ, 2004).

[6] K. J. Vahala, Optical microcavities, Nature (London) **424**, 839 (2003).

[7] R. K. Chang and A. L. Campillo, *Optical Processes in Microcavities* (World Scientific, Singapore, 1996).

[8] Y. Wu and X. Yang, Quantum theory for microcavity enhancement of second harmonic generation, J. Phys. B **34**, 2281 (2001).

[9] J. K. Day, M.-H. Chung, Y.-H. Lee, and V. M. Menon, Microcavity enhanced second harmonic generation in 2D MoS$_2$, Opt. Mater. Express **6**, 2360 (2016).

[10] A. Rodriguez, M. Soljačić, J. D. Joannopoulos, and S. G. Johnson, $\chi^{(2)}$ and $\chi^{(3)}$ harmonic generation at a critical power in inhomogeneous doubly resonant cavities, Opt. Express **15**, 7303 (2007).

[11] C. Xiong, W. Pernice, K. K. Ryu, C. Schuck, K. Y. Fong, T. Palacios, and H. X. Tang, Integrated GaN photonic circuits on silicon (100) for second harmonic generation, Opt. Express **19**, 10462 (2011).

[12] J. S. Levy, M. A. Foster, A. L. Gaeta, and M. Lipson, Harmonic generation in silicon nitride ring resonators, Opt. Express **19**, 11415 (2011).

[13] W. H. P. Pernice, C. Xiong, C. Schuck, and H. X. Tang, Second harmonic generation in phase matched aluminum nitride waveguides and micro-ring resonators, Appl. Phys. Lett. **100**, 223501 (2012).

[14] X. Guo, C.-L. Zou, and H. X. Tang, Second-harmonic generation in aluminum nitride microrings with 2500%/W conversion efficiency, Optica **3**, 1126 (2016).

[15] P. S. Kuo and G. S. Solomon, On- and off-resonance second-harmonic generation in GaAs microdisks, Opt. Express **19**, 16898 (2011).

[16] S. Mariani, A. Andronico, A. Lemaître, I. Favero, S. Ducci, and G. Leo, Second-harmonic generation in AlGaAs microdisks in the telecom range, Opt. Lett. **39**, 3062 (2014).

[17] C. Wang, M. J. Burek, Z. Lin, H. A. Atikian, V. Venkataraman, I.-C. Huang, P. Stark, and M. Lončar, Integrated high quality factor lithium niobate microdisk resonators, Opt. Express **22**, 30924 (2014).

[18] D. P. Lake, M. Mitchell, H. Jayakumar, L. F. Dos Santos, D. Curic, and P. E. Barclay, Efficient telecom to visible wavelength conversion in doubly resonant gallium phosphide microdisks, Appl. Phys. Lett. **108**, 031109 (2016).

[19] V. Ilchenko, A. Savchenkov, A. Matsko, and L. Maleki, Nonlinear Optics and Crystalline Whispering Gallery Mode Cavities, Phys. Rev. Lett. **92**, 043903 (2004).

[20] Y. Dumeige, Quasi-phase-matching and second-harmonic generation enhancement in a semiconductor microresonator array using slow-light effects, Phys. Rev. A **83**, 045802 (2011).

[21] G. Lin, J. U. Fürst, D. V. Strekalov, and N. Yu, Wide-range cyclic phase matching and second harmonic generation in whispering gallery resonators, Appl. Phys. Lett. **103**, 181107 (2013).

[22] P. S. Kuo, J. Bravo-Abad, and G. S. Solomon, Second-harmonic generation using 4-quasi-phasematching in a GaAs whispering-gallery-mode microcavity, Nat. Commun. **5**, 3109 (2014).

[23] J. U. Fürst, K. Buse, I. Breunig, P. Becker, J. Liebertz, and L. Bohatý, Second-harmonic generation of light at 245 nm in a lithium tetraborate whispering gallery resonator, Opt. Lett. **40**, 1932 (2015).

[24] J. Lin, Y. Xu, J. Ni, M. Wang, Z. Fang, L. Qiao, W. Fang, and Y. Cheng, Phase-Matched Second-Harmonic Generation in an On-Chip LiNbO$_3$ Microresonator, Phys. Rev. Appl. **6**, 014002 (2016).

[25] F. Leo, T. Hansson, I. Ricciardi, M. De Rosa, S. Coen, S. Wabnitz, and M. Erkintalo, Walk-Off-Induced Modulation Instability, Temporal Pattern Formation, and Frequency Comb Generation in Cavity-Enhanced Second-Harmonic Generation, Phys. Rev. Lett. **116**, 033901 (2016).

[26] M. Asano, S. Komori, R. Ikuta, N. Imoto, Ş. K. Özdemir, and T. Yamamoto, Visible light emission from a silica microbottle resonator by second- and third-harmonic generation, Opt. Lett. **41**, 5793 (2016).

[27] M. W. McCutcheon, J. F. Young, G. W. Rieger, D. Dalacu, S. Frédérick, P. J. Poole, and R. L. Williams, Experimental demonstration of second-order processes in photonic crystal microcavities at submilliwatt excitation powers, Phys. Rev. B **76**, 245104 (2007).

[28] K. Rivoire, Z. Lin, F. Hatami, W. T. Masselink, and J. Vučković, Second harmonic generation in gallium phosphide photonic crystal nanocavities with ultralow continuous wave pump power, Opt. Express **17**, 22609 (2009).

[29] M. Galli, D. Gerace, K. Welna, T. F. Krauss, L. O'Faolain, G. Guizzetti, and L. Claudio Andreani, Low-power continuous-wave generation of visible harmonics in silicon photonic crystal nanocavities, Opt. Express **18**, 26613 (2010).

[30] G. Shambat, K. Rivoire, J. Lu, F. Hatami, and J. Vučković, Tunable-wavelength second harmonic generation from GaP photonic crystal cavities coupled to fiber tapers, Opt. Express **18**, 12176 (2010).

[31] S. Buckley, M. Radulaski, K. Biermann, and J. Vučković, Second harmonic generation in photonic crystal cavities in (111)-oriented GaAs, Appl. Phys. Lett. **103**, 211117 (2013).

[32] S. Buckley, M. Radulaski, J. Petykiewicz, K. G. Lagoudakis, J.-H. Kang, M. Brongersma, K. Biermann, and J. Vučković, Second-Harmonic Generation in GaAs Photonic Crystal Cavities in (111)B and (001) Crystal Orientations, ACS Photonics **1**, 516 (2014).

[33] T. K. Fryett, K. L. Seyler, J. Zheng, C.-H. Liu, X. Xu, and A. Majumdar, Silicon photonic crystal cavity enhanced second-harmonic generation from monolayer WSe$_2$, 2D Mater. **4**, 015031 (2016).

[34] J. U. Fürst, D. V. Strekalov, D. Elser, M. Lassen, U. L. Andersen, C. Marquardt, and G. Leuchs, Naturally Phase-Matched Second-Harmonic Generation in a Whispering-Gallery-Mode Resonator, Phys. Rev. Lett. **104**, 153901 (2010).

[35] Ş. K. Özdemir, J. Zhu, X. Yang, B. Peng, H. Yilmaz, L. He, F. Monifi, S. H. Huang, G. L. Long, and L. Yang, Proc. Natl. Acad. Sci. USA **111**, E3836 (2014).

[36] L. He, Ş. K. Özdemir, J. Zhu, and L. Yang, Ultrasensitive detection of mode splitting in active optical microcavities, Phys. Rev. A **82**, 053810 (2010).

[37] V. Huet, A. Rasoloniaina, P. Guillemé, P. Rochard, P. Féron, M. Mortier, A. Levenson, K. Bencheikh, A. Yacomotti, and Y. Dumeige, Millisecond Photon Lifetime in a Slow-Light Microcavity, Phys. Rev. Lett. **116**, 133902 (2016).

[38] M. Asano, Ş. K. Özdemir, W. Chen, R. Ikuta, L. Yang, N. Imoto, and T. Yamamoto, Controlling slow and fast light and dynamic pulse-splitting with tunable optical gain in a whispering-gallery-mode microcavity, Appl. Phys. Lett. **108**, 181105 (2016).

[39] F. Lei, B. Peng, Ş. K. Özdemir, G. L. Long, and L. Yang, Dynamic Fano-like resonances in erbium-doped whispering-gallery-mode microresonators, Appl. Phys. Lett. **105**, 101112 (2014).

[40] Y. Jiao, H. Lü, J. Qian, Y. Li, and H. Jing, Nonlinear optomechanics with gain and loss: Amplifying higher-order sideband and group delay, New J. Phys. **18**, 083034 (2016).

[41] V. V. Konotop, J. Yang, and D. A. Zezyulin, Nonlinear waves in $\mathcal{PT}$-symmetric systems, Rev. Mod. Phys. **88**, 035002 (2016).

[42] L. Ge and R. El-Ganainy, Nonlinear modal interactions in parity-time ($\mathcal{PT}$) symmetric lasers, Sci. Rep. **6**, 24889 (2016).

[43] L. Feng, Z. J. Wong, R.-M. Ma, Y. Wang, and X. Zhang, Single-mode laser by parity-time symmetry breaking, Science **346**, 972 (2014).

[44] H. Hodaei, M.-A. Miri, M. Heinrich, D. N. Christodoulides, and M. Khajavikhan, Parity-time-symmetric microring lasers, Science **346**, 975 (2014).

[45] H. Hodaei, M. A. Miri, A. U. Hassan, W. E. Hayenga, M. Heinrich, D. N. Christodoulides, and M. Khajavikhan, Parity-time-symmetric coupled microring lasers operating around an exceptional point, Opt. Lett. **40**, 4955 (2015).

[46] H. Hodaei, M.-A. Miri, A. U. Hassan, W. E. Hayenga, M. Heinrich, D. N. Christodoulides, and M. Khajavikhan, Single mode lasing in transversely multi-moded PT-symmetric microring resonators, Laser Photonics Rev. **10**, 494 (2016).

[47] B. Peng, Ş. K. Özdemir, F. Lei, F. Monifi, M. Gianfreda, G. L. Long, S. Fan, F. Nori, C. M. Bender, and L. Yang, Parity-time-symmetric whispering-gallery microcavities, Nat. Phys. **10**, 394 (2014).

[48] L. Chang, X. Jiang, S. Hua, C. Yang, J. Wen, L. Jiang, G. Li, G. Wang, and M. Xiao, Parity-time symmetry and variable optical isolation in active-passive-coupled microresonators, Nat. Photonics **8**, 524 (2014).

[49] R. El-Ganainy, M. Khajavikhan, and L. Ge, Exceptional points and lasing self-termination in photonic molecules, Phys. Rev. A **90**, 013802 (2014).

[50] K.-H. Kim, M.-S. Hwang, H.-R. Kim, J.-H Choi, Y.-S. No, and H.-G. Park, Direct observation of exceptional points in coupled photonic-crystal lasers with asymmetric optical gains, Nat. Commun. **7**, 13893 (2016).

[51] A. U. Hassan, H. Hodaei, M. Miri, M. Khajavikhan, and D. N. Christodoulides, Nonlinear reversal of PT symmetric phase transition in a system of coupled semiconductor microring resonators, Phys. Rev. A **92**, 063807 (2015).

[52] J. Ren, H. Hodaei, G. Harari, A. U. Hassan, W. Chow, M. Soltani, D. N. Christodoulides, and M. Khajavikhan, Ultrasensitive micro-scale parity-time-symmetric ring laser gyroscope, Opt. Lett. **42**, 1556 (2017).

[53] D. Walls and G. Milburm, *Quantum Optics* (Springer, Berlin, 1994).

[54] C. W. Gardiner and P. Zoller, *Quantum Noise* (Springer, Berlin, 2004).

[55] B. Peng, S. K. Oezdemir, J. Zhu, and L. Yang, Photonic molecules formed by coupled hybrid resonators, Opt. Lett. **37**, 3435 (2012).

[56] X. Guo, C. Zou, C. Schuck, H. Jung, R. Cheng, and H. X. Tang, Parametric down-conversion photon pair source on a nanophotonic chip, Light Sci. Appl. **6**, e16249 (2017).

[57] The down-conversion process is neglected in the so-called undepleted pump limit. This treatment leads to incorrect results in the limit of high conversion efficiency. Here, our scheme fully incorporates such a competing effect of optical stimulated down-conversion in Eqs. (11)–(13).

[58] See the supplementary material accompanying Ref. [14].

[59] H. Jing, Ş. K. Özdemir, X.-Y. Lü, J. Zhang, L. Yang, and F. Nori, $\mathcal{PT}$-Symmetric Phonon Laser, Phys. Rev. Lett. **113**, 053604 (2014).

[60] J. Zhang, B. Peng, Ş K. Özdemir, Y.-X. Liu, H. Jing, X.-Y. Lü, Y.-L. Liu, L. Yang, and F. Nori, Giant nonlinearity via breaking parity-time symmetry: A route to low-threshold phonon diodes, Phys. Rev. B **92**, 115407 (2015).

[61] X.-Y. Lü, H. Jing, J.-Y. Ma, and Y. Wu, $\mathcal{PT}$-Symmetry-Breaking Chaos in Optomechanics, Phys. Rev. Lett. **114**, 253601 (2015).

[62] Y.-L. Liu and Y.-X. Liu, Energy localization and ground-state cooling of mechanical resonator from room temperature in optomechanics using a gain cavity, arXiv:1609.02722.

[63] S. Ke, B. Wang, C. Qin, H. Long, K. Wang, and P. Lu, Exceptional points and asymmetric mode switching in plasmonic waveguides, J. Lightwave Technol. **34**, 5258 (2016).